International Journal of Hydrogen Energy 235 (2026) 155073

Contents lists available at ScienceDirect

International Journal of Hydrogen Energy

journal homepage: www.elsevier.com/locate/he

Towards green steel from hydrogen-based direct reduction of low-grade iron ores: Techno-economic and greenhouse gas emissions assessment

João Miguel Margutti [a], Matthias Schiedeck [a], Philipp Morsch [a,*], Sarah Deutz [a], Sabrine Khadhraoui [b], Thomas Wolfinger [c], Andreas Peschel [a,d]

[a] Forschungszentrum Jülich GmbH, Institute for a sustainable Hydrogen Economy (IHE), Jülich, Germany
[b] SMS group GmbH, R&D - Physics and Processes (RDZP), Mönchengladbach, Germany
[c] Paul Wurth S.A., CoC Iron - Process & Technology, Luxembourg
[d] RWTH Aachen University, Aachener Verfahrenstechnik, Process and Plant Engineering for Chemical Hydrogen Storage, Aachen, Germany

ARTICLE INFO

Keywords:
Hydrogen
Green steel
Low-grade iron ores
Direct reduction of iron
Electric arc furnace
Electric smelting furnace

ABSTRACT

Strict feedstock purity and pelletizing requirements challenge shaft-furnace, hydrogen-based direct reduction of iron (H_2DRI) with electric arc furnace (EAF) steelmaking. Fluidized-bed (FB) reactors eliminate pellet use by reducing fine ore; however, high DRI metallization risks reactor de-fluidization. The novel electric smelting furnace-basic oxygen furnace (ESF-BOF) configuration enables splitting iron reduction between FB and ESF to prevent de-fluidization. This study compares FBH$_2$DRI-EAF vs. FBH$_2$DRI-ESF-BOF, investigating the impact of ore grade and DRI metallization on levelized cost of steel (LCOS) and GHG emissions. Despite lower feedstock cost, processing low-grade ore via FBH$_2$DRI-EAF raises LCOS by 16 %. Conversely, FBH$_2$DRI-ESF-BOF leverages lower feedstock costs effectively. As global ore purity decreases, this advantage grows increasingly relevant. Elevated GHG penalties have limited economic impact, but affordable green reductant supply is essential for cost minimization. At 1.5 €/kgH$_2$ and 80 €/tCO$_2$e penalty (best case), the LCOS varies from 565 €/tLS to 578 €/tLS depending on DRI metallization.

1. Introduction

In 2024, approximately 1.89 Gt of crude steel (CS) were produced worldwide, with average gate-to-gate CO_2 emissions intensity of 1.92 tCO$_2$/tCS [1] - representing 9.8 % of the global total of 37.01 GtCO$_2$ [2]. The blast furnace-basic oxygen furnace (BF-BOF) route made up 70.4 % of the produced steel volume [1]. In this route, liquid-phase iron ore reduction with metallurgical coke takes place inside the BF, producing a hot metal with high carbon content of up to 4.5 wt.% [3]. Non-metallic impurities contained in the iron ore source, commonly referred to as gangue, are separated as a liquid slag phase. After water quenching, granulated blast furnace slag offsets the clinker demand in cement production, reducing greenhouse gas (GHG) emissions [4]. In a subsequent BOF, the excessive carbon content in the hot metal is tailored to the desired level via oxy-combustion, yielding crude steel. This route results in a high cradle-to-gate GHG emissions intensity of 2.66 tCO$_2$e/tCS [5]. Given the steel industry's long-term investment cycles, it is imperative to rapidly scale up technologies for decarbonize steel production.

Green steel will heavily rely on low-carbon hydrogen for the direct reduction (DR) process [6]. Direct reduced iron (DRI) is produced via solid-phase reduction in a shaft furnace using an H_2-containing synthesis gas as reductant. The DRI intermediate is subsequently charged into a steelmaking furnace, typically an electric arc furnace (EAF), to yield crude steel. To date, this synthesis gas mixture comes predominantly from steam reforming of natural gas, which emits a considerable amount of CO_2. Depending on the electricity mix, the process is able to reach 1.27 tCO$_2$/tCS, cutting the BF-BOF's carbon footprint by 55 % [7]. Direct reduction using 100 % green H_2 (H_2DRI), followed by a renewables-powered EAF has the potential to deliver near-zero emissions steel [8]. While not yet deployed at a commercial scale, the H_2DRI-EAF process route leverages industrial technologies and state-of-the-art equipment, offered by established players [9,10]. Conversely, other scientifically promising low-carbon technologies, such as electro-winning [11], molten-oxide electrolysis [12] and hydrogen plasma-based reduction of iron ore [13] or red mud [14] still lack the technological maturity to be considered for commercial projects in the short to medium term. So, is H_2DRI-EAF indeed the best alternative to produce decarbonized steel?

Certainly, this process concept has captured interest across a myriad of studies in the literature. Vogl et al. [15] published a pioneering work,

* Corresponding author.
E-mail address: p.morsch@fz-juelich.de (P. Morsch).

https://doi.org/10.1016/j.ijhydene.2026.155073
Received 9 February 2026; Received in revised form 12 April 2026; Accepted 15 April 2026
Available online 24 April 2026

Nomenclature

CS	Crude steel
BOF	Basic oxygen furnace
BF	Blast furnace
GHG	Greenhouse gas
DR	Direct reduction
DRI	Direct reduced iron
EAF	Electric arc furnace
DRP	Direct reduction plant
GHG	Greenhouse gas
CFB	Circulating fluidized bed
MD	Metallization degree of DRI
ESF	Electric smelting furnace
LS	Liquid steel
CapEx	Capital expenditure
OpEx	Operational expenditure
LOI	Loss on ignition
PFD	Process flow diagram
CSTR	Continuously stirred tank reactor
CALPHAD	Computer Coupling of Phase Diagrams and Thermochemistry
LCOS	Levelized cost of steel
O&M	Operations & maintenance
IEA	International Energy Agency
LCOH	Levelized cost of hydrogen
HRC	Hot-rolled coil

assessing reasonable carbon abatement costs compared to BF-BOF relining, based on simplified mass and energy flow calculations. Müller et al. [16] provide a much more detailed model in AspenPlus™, allowing them to reduce empirical assumptions and investigate waste heat recovery, e.g. in combination with a high-temperature solid-oxide water electrolyzer. Building upon their work, Jacobasch et al. [17] introduced a bottom-up economic evaluation and examined the gradual transition from NG to H_2 as reducing gas. The break-even cost point between H_2 and natural gas was the object of study by Rosner et al. [18]. Depending on whether H_2 is used for both heating and reduction, only for reduction, or if there is heat integration with the EAF, they found break-even procurement costs for hydrogen in the range of $1.63\,\$/kgH_2$ to $1.70\,\$/kgH_2$. More recently, Scaccabarozzi et al. [19] shed light on possible thermal and chemical integration approaches between direct reduction and high-temperature solid-oxide electrolysis, analyzing system performance even under off-design operation due to an intermittent renewable energy supply. Along similar lines, Immonen et al. [20] compare the integration of different electrolyzers with the direct reduction plant (DRP) and contemplate the use of waste heat from the EAF. Despite being indeed a promising route, H_2DRI-EAF still entails some major challenges.

On the one hand, the current DRI shaft furnace design requires pelletized ore [21]. Pelletizing is an energy-intensive ($424\,MJ/t_{Pellet}$ [22]) process reliant on high-temperature firing of fuel oil and bears significant environmental impact beyond GHG emissions, such as acidification and ozone layer depletion [23]. To circumvent the use of pellets, shaft furnaces can be replaced with fluidized-bed reactors, as the latter are able to reduce fine ore. H_2-induced fluidized-bed reduction of fines and ultra-fines have been extensively characterized in the literature [24–26]. Recently, commercial fluidized-bed technologies were thoroughly analyzed [27]. Among these, we highlight the Circored® process, where fine ores are pre-reduced in a one-stage circulating fluidized-bed (CFB) reactor to achieve a DRI metallization degree (*MD*) of 70 %, before final reduction until 93 % to 95 % takes place inside a bubbling fluidized bed [28]. Challenges of the fluidized-bed reduction include an inhomogeneous fluidization behavior due to broad particle size distributions. Particularly, sticking, i.e., solid particle agglomeration compromising reactor fluidization, becomes critical with increasing reaction temperatures and DRI metallization degrees [27].

On the other hand, direct reduction does not enable gangue removal through the liquid slag as in BF ironmaking. Consequently, the DRI will carry major impurities from the iron ore feedstock into the melt shop [29]. The EAF was primarily designed for secondary steel production, i.e., melting steel scrap, a refined, metallic feedstock free of gangue minerals [30]. Most of the above cited H_2DRI-EAF studies take literature correlations or perform simplified energy balance calculations to estimate the energy consumption in the EAF. By doing so, they either completely neglect or overly simplify the ore-specifics in EAF steelmaking. Elevated gangue levels impact the EAF's energy demand, besides producing high slag volumes, which the EAF is not well equipped to handle [31,32]. Its slag phase requires an FeO content of ca. 20 wt.% to 25 wt.% to control viscosity and enable foaming [33], meaning iron losses are higher the more gangue is present. Hence, DR-grade iron ores with minimum Fe content of ca. 67 % are strongly preferred; for reference, they represent merely 4 % of global ore exports [34].

The electric smelting furnace (ESF), also known as open-bath furnace is better suited to process lower-grade iron ores [35,36]. It requires carbon to fulfill the iron ore reduction and carburize the hot metal intermediate, which is converted into crude steel preserving the existing downstream BOF. Due to the ESF's reducing atmosphere, the iron losses (as FeO) to the slag are greatly reduced in comparison to the EAF. An additional advantage is the co-production of a BF-like slag phase, which will also likely find its use in the cement industry. As, currently, ESF technology is mostly deployed in ferroalloy production, there are few studies on it available in the context of ferrous metallurgy [37–40].

Recently, Rahbari et al. [40] compared the cost performance of shaft furnace and fluidized bed-based DRI processes, respectively coupled to EAF and ESF-BOF steelmaking, considering different levels of ore beneficiation. Their work was conducted in HSC Sim®, which is not based on rigorous metallurgical thermodynamics. Additionally, they assume that DRI reaches 100 % metallization inside a fluidized-bed reactor, thus not considering the practical constraints imposed by the intensified sticking at elevated DRI metallization levels. This raises the question of how intentionally splitting the reduction between the H_2-based fluidized bed and the carbon-based ESF would influence the overall process route's performance. To the best of the authors' knowledge, no end-to-end assessment of the economics and GHG emissions of the H_2DRI-ESF-BOF route for varying DRI metallization levels, grounded in detailed metallurgical thermodynamics, is available to date.

In this work, we investigate the economics and GHG emissions of processing low-grade ores into crude liquid steel (LS) via H_2DRI and EAF or ESF-BOF. Our novelty lies in combining the following contributions:

- Conceptual design and process simulation of CFB-based H_2DRI production from fine magnetitic ore, including a bottom-up methodology to estimate the plant's capital and operational expenditure (CapEx, OpEx) upon varying DRI metallization degree.
- Metallurgical simulation of EAF and ESF-BOF steelmaking, providing insights into volumetric requirements and generating thermodynamically consistent mass and energy balances for two different iron ore compositions.
- For the H_2DRI-ESF-BOF route, we compute the thermodynamics over a wide DRI metallization range from 65 % to 95 %. This allows flexibly splitting the iron ore reduction between the CFB and the ESF (e.g. to prevent sticking).
- Sensitivity of the levelized cost of steel and GHG emissions against varying metallization degrees achieved during the H_2DRI process, as well as the variation of H_2 and GHG costs.

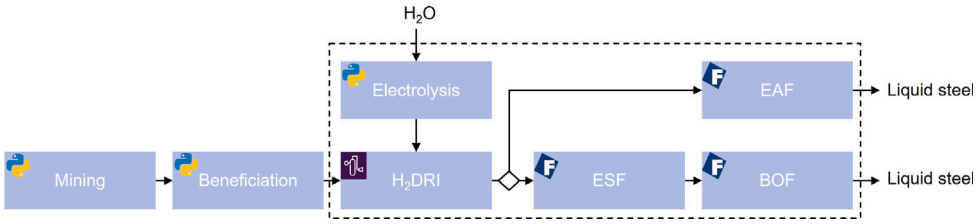

Fig. 1. Block flow diagram of the system modeled in this work, with the considered balance envelope for the gate-to-gate GHG emissions represented as dashed line. H_2DRI: H_2-based direct reduction of iron ore; ESF: electric smelting furnace; BOF: basic oxygen furnace; EAF: electric arc furnace.

Table 1
Composition of DR-grade (left) and BF-grade (right) iron ore concentrate samples from South America.

Component	DR-grade mass fraction, wt.%	BF-grade mass fraction, wt.%
Fe_3O_4	82.5	66.1
Fe_2O_3	5.1	10.9
SiO_2	4.0	9.7
Al_2O_3	1.7	3.1
MgO	0.9	1.2
CaO	0.8	4.0
LOI (H_2O)	5.0	5.0

2. Methodology

2.1. Process modeling

We model a vertically integrated facility for production of green steel, including hydrogen generation, iron ore preparation (mining and beneficiation), direct reduction and steelmaking via EAF or ESF-BOF as part of the battery limits (Fig. 1).

2.1.1. Hydrogen generation plant

Hydrogen generation is modeled with a high level of abstraction, based on previous work [41]. It is produced via pressurized alkaline electrolysis, with a specific energy consumption of 51.8 MWh/tH_2 and specific demineralized water consumption of 8.9 l/tH_2.

2.1.2. Iron ore preparation plant

Iron ore preparation is modeled with a high level of abstraction, based on previous work [22]. It comprises local mining and beneficiation. These units are oversized to account for material losses of crude ore, ensuring that the required amount of DR-grade or BF-grade ore is delivered to the direct reduction plant (DRP). Pelletizing is excluded, as the CFB reactor processes fine ore. We assume that iron ore is locally available with an initial Fe content as low as 30 % and can be beneficiated, respectively, into BF-grade and DR-grade iron ore concentrates. Their respective Fe contents are 67 wt.% (DR-grade) and 58 wt.% (BF-grade) on a dry basis. The compositions of the two South American samples, provided by our industrial collaborator, can be found in Table 1, where the loss on ignition (LOI) is modeled as H_2O. A more thorough description of the iron ore preparation model is provided in Supplementary Information SI1.

2.1.3. Direct reduction plant

Ironmaking via direct reduction is modeled in detail using the commercial software AVEVA Process Simulation™, with a simplified process flow diagram (PFD) represented in Fig. 2. In the direct reduction plant model, fluid phase behavior is modeled using the Soave–Redlich–Kwong equation of state, whereas iron, its oxides and the gangue components are treated as non-equilibrium solids. As such, the latter experience heating, cooling and chemical conversions according to a defined stoichiometry. We refrain from Gibb's free energy-driven chemical conversions, further physical–chemical interactions and structural phase transitions at the relevant process conditions. In an electrically heated rotary kiln, the iron ore feed is dried, while magnetite (Fe_3O_4) is simultaneously pre-oxidized to hematite (Fe_2O_3) with air. Limiting the water content in the reducing gas is crucial, as water is known to negatively impact reduction thermodynamics and kinetics [42–44]. Pre-oxidation is advantageous because hematite exhibits superior reducibility and fluidization behavior compared to magnetite [45,46]. The rotary kiln is considered to be equipped with a standard gas–solid separation system, such as a settling chamber, cyclone separator or internal weirs to remove the entrained ore particles from the hot off-gas stream. After exiting the rotary kiln, iron ore is injected into a CFB reactor system with H_2-rich reductant, which has been pre-heated by a sequence of heat exchangers, to reach the desired reactor inlet temperature. Hematite is fully reduced into wüstite, according to Eq. (1):

$$Fe_2O_3 + H_2 \rightarrow 2\,FeO + H_2O, \tag{1}$$

with the latter partially converted into metallic iron as shown in Eq. (2):

$$FeO + H_2 \rightarrow Fe + H_2O. \tag{2}$$

Hydrogen is dosed in stoichiometric excess to minimize the water content in the top gas outlet stream, as higher water content increases the gas oxidation potential, i.e., higher tendency that iron is converted back to its oxides. To determine the allowable top gas water content, the Baur-Glässner diagram [40] was consulted. We chose to limit the top gas water content to 26 wt.%, as this lies close to the thermodynamic limit, upon which Fe formation is still favored across all temperatures studied in this work. In our model, we control the top gas water content indirectly, by specifying an effective stoichiometric number at the CFB system's inlet, SN_{eff}, of 4. The mathematical definition of SN_{eff} is based on the stoichiometry of the involved reactions (see Eqs. (1) and (2)) and presented in Eq. (3):

$$SN_{eff} = \frac{\dot{N}_{H_2}}{(1 + 2 \cdot MD) \cdot \dot{N}_{Fe_2O_3}}. \tag{3}$$

Here, $\dot{N}$ represents the molar flow of the reactant in the subscript, whereas MD the metallization degree achieved by the DRI product. In our model, MD is calculated according to Eq. (4):

$$MD = \frac{\dot{M}_{Fe}}{\dot{M}_{Fe} + z_{Fe/FeO} \cdot \dot{M}_{FeO}}, \tag{4}$$

where $\dot{M}$ denotes the mass flow of the solid compound in the subscript and $z_{Fe/FeO}$ the mass content of iron inside wustite. MD is determined by the partial conversion of wüstite to metallic iron (Eq. (2)), as no further oxidized iron species are present in DRI.

Reduction kinetics is known to decelerate drastically as the metallization degree increases [47]. An excessively long residence time inside one reactor would require unreasonable equipment sizes to achieve high metallization. Therefore, we foresee a sequential cascade of equally dimensioned CFBs according to Table 2. The kinetic behavior of the CFB cascade is approximated as a series of identical continuously stirred tank reactors (CSTRs) based on the kinetic measurements

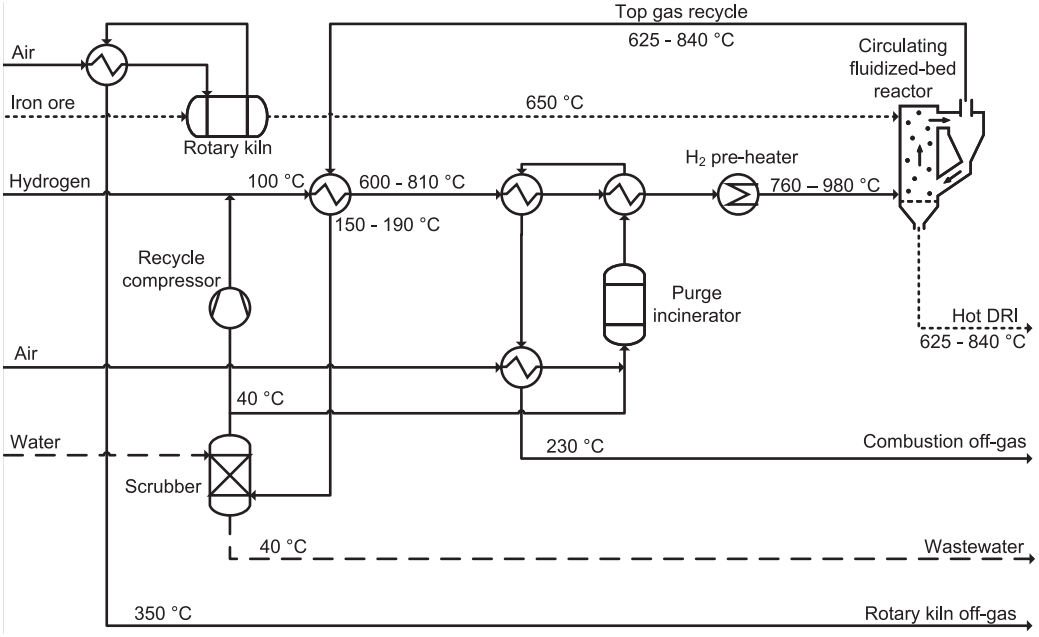

Fig. 2. Simplified process flow diagram of the direct reduction plant. Solid lines represent gaseous streams, dashed lines represent liquid streams and dotted lines represent solid material flows.

Table 2
CFB cascade configuration according to DRI metallization degree.

MD range in %	#CFB
$0 < MD \leq 70$	1
$70 < MD \leq 87$	2
$87 < MD \leq 95$	3

by Habermann [48] for the San Isidro ore. To estimate the riser tube dimensions, we couple kinetics (residence time) with fluid dynamics (flow velocity), subject to a constructability constraint (height/diameter ratio of 5). The significant entrainment velocity U_{se} for the analyzed gas–solid system is imposed as minimum flow velocity to accomplish fast fluidization, i.e., CFB conditions [49]. For a mean ore particle diameter of 300 µm, U_{se} is determined as a function of the Archimedes number, deploying the correlation by Abba et al. [50]. This results in a system of non-linear algebraic equations that is solved numerically to yield the required solid recirculation rate, the actual gas–solid volume flow and the riser dimensions. The reader is referred to Supplementary Information SI2 for a detailed description of the CFB dimensioning approach. Additionally, for each CFB riser tube, convective heat loss is calculated using Newton's law of cooling, with a fixed heat transfer coefficient of $\alpha = 5\,\mathrm{W/(m^2\,K)}$, and the actual temperature difference between the reactor and the environment $\Delta T = T_{\mathrm{DRI}} - T_{\mathrm{amb}}$. The pressure loss per CFB stage is estimated at 0.8 bar, approximately equivalent to the geodetic pressure difference for the fluidized system at an average bed porosity of 64 % over a height of 10 m.

DRI exits the reactor after reaching a defined metallization degree. A fraction of 5 % of the DRI product is diverted as dust, which is captured by a filter system. Assuming spontaneous, full re-oxidation of iron to hematite, this dust is recycled as iron ore feed to prevent solid disposal costs. The H_2-rich top gas containing water is also recirculated. After pre-heating the hydrogen inlet stream, the top gas is further cooled via direct injection of cooling water in a scrubber. The liquid drain is disposed to a wastewater treatment unit outside of the battery limits. A small fraction of the gas recycle is purged to prevent accumulation of inert components inside the reaction loop. After combustion of the purge stream, the hot burner off-gas also preheats the hydrogen feed stream in a cascade of two feed-effluent heat exchangers to prevent thermal stress arising from the high temperature differences. The largest part of the gas recycle stream is compressed to the initial pressure and mixed with the hydrogen make-up.

2.1.4. Steelmaking plant

Herein, steelmaking denotes either an EAF or a combination of ESF-BOF, in which DRI is converted into liquid steel. An in-depth description of the involved computational steps and data flow between modules is presented in Supplementary Information SI3. To capture the complex (multi-component, vapor–liquid–liquid–solid) equilibrium thermodynamics involved, we make use of the CALPHAD methodology (Gibb's free energy minimization) inside the FactSage® 8.3 environment. The thermodynamic databases used were FactPS for the (ideal) off-gas phases, FToxid for the slag phases, and FTmisc for the hot metal and liquid steel phases. Our modeling approach does not consider any kinetic effects involved in the steelmaking plant. We assume a temperature loss of 50 °C between the direct reduction and the steelmaking plants, reflecting an optimistic estimate for an efficient solid conveyor system between the direct reduction and steelmaking plants, such as MIDREX's HOTLINK® [51]. The steelmaking plant produces mild steel, with a carbon content in the range of 0.01 wt.% to 0.08 wt.%. Note that this is on the lower end of the interval 0.01 % to 0.25 % reported in the literature [52].

The EAF conditions are based on previous work [33,40,53,54]. DRI with a high metallization degree of 95 % is charged alongside fluxes, carbon (coke plus graphite electrode consumption), oxygen and scrap. We do not consider the option of supplying DRI with a lower metallization degree to the EAF. Scrap is added in the same proportion as required in the BOF to improve the comparability between the H_2DRI-EAF and the H_2DRI-ESF-BOF routes. Liquid steel is tapped at 1600 °C and atmospheric pressure. Because the EAF is an open vessel, the process incurs two heat penalties: air infiltration at a rate of 100 kg/tLS and miscellaneous thermal losses of 49 kW h/tLS. Moreover, an electrical efficiency of 90 % is assumed, representing the losses associated with converting electrical energy into thermal arc energy, i.e., transformer, cabling, and electrode-circuit losses. Additional process specifications are summarized in Table 3, with more information provided in Supplementary Information SI3.1.

Table 3
EAF process specifications.

Specification	Target	Tolerance	Unit	Manipulated variable
Mass ratio CaO:SiO_2 in slag	2.00	0.05	–	CaO input
Mass fraction MgO in slag	7.0	0.1	wt.%	MgO input
Mass fraction FeO in slag	25.0	0.5	wt.%	O_2 input
Mass fraction C in liquid steel	0.045	0.035	wt.%	O_2 input
Mass ratio CH_4 input	4.00	0.01	kg/tLS	CH_4 input
Mass ratio C input	14.00	0.05	kg/tLS	C input
Scrap input ratio	212	1	kg/tLS	Scrap input

The ESF conditions are largely based on previous work [39,40,55]. DRI with varying metallization degree is charged alongside fluxes and carbon. We consider an inhomogeneous temperature profile with higher slag temperatures, increased slag basicity, and a high Si content in the hot metal phase. To capture this behavior while retaining a single-equilibrium-zone calculation in FactSage®, a uniform temperature is specified for thermodynamic computations: 1600 °C for the DR-grade (lower SiO_2) and 1500 °C for the BF-grade (higher SiO_2) ore. Note that the different temperatures reflect the influence of the SiO_2 content of the DRI charge and are selected to ensure that the Si content of the hot metal can reach the desired level upon addition of C and CaO. In a subsequent step, the energy balance for the hot metal phase in the ESF is adjusted by subtracting the amount of heat that would correspond to a tapping temperature of 1400 °C. No air infiltration is accounted for, as the ESF is regarded as a hermetically sealed vessel. Moreover, we assume an electric efficiency of 90 %. Additional process specifications are summarized in Table 4, with more information provided in Supplementary Information SI3.2. The ESF model proved to be in good agreement with previous investigations in the literature [55,56] and insights provided by our industrial collaborator.

The BOF conditions are based on previous work [57–59]. Hot metal exiting the ESF at 1400 °C is charged alongside fluxes, oxygen and scrap at atmospheric pressure. Scrap, assumed to be 100 % Fe, is added in amounts that allow for thermal dissipation to be constrained to 10 kW h/tLS (see Table 5). The tapping temperature of 1650 °C is chosen at atmospheric pressure. Additional process specifications are summarized in Table 5, with more information provided in Supplementary Information SI3.3.

2.2. Evaluation metrics

2.2.1. Economics

The levelized cost of steel (LCOS) is determined using a discounted cashflow calculation, outlined in Eq. (5):

$$\mathrm{LCOS} = \frac{\sum_{i=1}^{N} \frac{CapEx_i + OpEx_i}{(r+1)^{i-1}}}{\sum_{i=1}^{N} \frac{M_{LS}}{(r+1)^{i-1}}}. \quad (5)$$

Here, $CapEx_i$ and $OpEx_i$ are the capital and operational expenditures at project year i; M_{LS} is the annual liquid steel output and r is the real (inflation-adjusted) discount rate of 10 %.

The CapEx of the integrated facility is estimated on a conceptual level using a hybrid approach. For the alkaline electrolysis, a specific CapEx of 2310 €/kW [60] is linearly scaled to the required plant size, which is in line with the current modular plant design chosen for large-scale electrolyzer plants (see Supplementary Information SI5). The CapEx of the iron ore preparation plant, based on literature data, accounts for logarithmic mass losses during the ore beneficiation step (see Supplementary Information SI1) [22]. The CapEx of the direct reduction plant is estimated using a bottom-up approach relying on equipment-specific correlations from literature [61]. The approach is detailed in Supplementary Information SI4. The reference CapEx values for the EAF, ESF, and BOF are taken from literature [22], which reports that the specific CapEx for EAF (in €/(tLS/y)) and ESF (in €/(tHM/y)) are equal. This likely reflects a best-guess estimate, as very few ESFs are in commercial use for ferrous applications and reliable data are scarce. To fairly compare the EAF and ESF technologies—especially for processing DRI charges of varying purity—it is necessary to adopt a volume-based approach that accounts for differences in specific slag formation and phase density. The densities of the hot metal (7071 kg/m^3) and liquid steel (7905 kg/m^3) phases are taken from FactSage®; the densities of EAF (3014 t/m^3) and ESF (2749 t/m^3) slag phases are estimated using a widespread, open-source spreadsheet tool from literature [62]. Accordingly, we establish the EAF operated with DR-grade feedstock as the reference case and convert the reported literature value of 329 €/(tLS/y) to a volumetric basis as 1507 €/(m^3/y) (slag formation 276 kg/tLS, overall 4.6 tLS/m^3). This value is then scaled using a degression exponent of 0.65 to estimate the CapEx of the EAF based on BF-grade feedstock, as well as the CapEx for the ESF based on DR-grade and BF-grade feedstock.

Table 4
ESF process specifications.

Specification	Target	Tolerance	Unit	Manipulated variable
Mass ratio CaO:SiO_2 in slag	1.67 (DR) 1.28 (BF)	0.01	–	CaO input
Mass fraction C in hot metal	4.00	0.05	wt.%	C input
Mass fraction Si in hot metal	0.80	0.01	wt.%	C and CaO input

Table 5
BOF process specifications.

Specification	Target	Tolerance	Unit	Manipulated variable
Mass ratio CaO:SiO_2 in slag	3.50	0.05	–	CaO input
Mass fraction MgO in slag	7.0	0.1	wt.%	MgO input
Mass fraction FeO in slag	25.0	0.5	wt.%	O_2 input
Mass fraction C in liquid steel	0.045	0.035	wt.%	O_2 input
Scrap input ratio	212	1	kg/tLS	Scrap input

The full CapEx is distributed along the first 4 project years according to a defined schedule, whereas the OpEx runs constantly from the 5th through the 24th year. The OpEx consists of both fixed and variable components. Fixed OpEx includes a labor cost of 53.2 €/tLS [15], besides an annual operations and maintenance (O&M) allowance set at 3 % of the total CapEx. Variable OpEx covers electricity, feedstock and other utilities. The complete set of economic parameters, including the specific utility costs and further explanations is provided in Supplementary Information SI5.

2.2.2. Greenhouse gas emissions

We follow a gate-to-gate approach, focusing on Scope 1 (direct) and Scope 2 (indirect, energy-related) emissions within the process battery limits. Scope 3 emissions are excluded, as they lie outside the system boundaries of this study and would only be considered in cradle-to-gate or cradle-to-grave analyses. Note that only Scope 1 emissions contribute directly to the levelized cost of steel, with Scope 2 emission penalties assumed to be embedded in the purchased electricity price.

H_2 generation via alkaline water electrolysis produces no direct GHG emissions. Furthermore, the direct reduction plant relies on H_2 as reducing agent and, as such, does not release any direct GHG emissions. The steelmaking furnaces (EAF, ESF) require carbon as chemical feedstock for reduction and carburization. While biogenic carbon (i.e., biochar) is theoretically feasible, there are significant challenges hampering its technical implementation and large-scale deployment [63,64]. For this reason, we consider fossil carbon, with furnace off-gas CO and CO_2 included in Scope 1 emissions (assuming stoichiometric CO to CO_2 conversion). As fossil carbon is considered to constitute 100 % C, other minor fossil emissions (e.g., N_2O) are deemed out of scope.

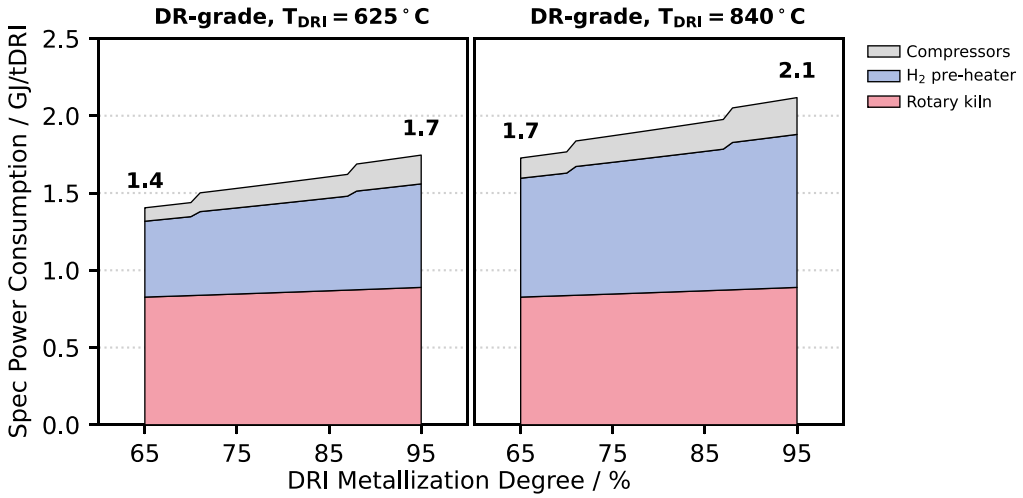

Fig. 3. Specific electricity consumption of the H_2-based DRP fed with DR-grade ore against different outlet temperatures and metallization degrees. DRP outlet temperatures: 625 °C (left); 840 °C (right).

Scope 2 emissions originate from the energy consumption of electrolysis, direct reduction and EAF/ESF units. As electricity is the sole external energy input, no additional Scope 2 emissions apply. We perform sensitivity studies to quantify the influence of the electricity-related GHG intensity on the specific GHG emissions of steel.

Although there is no standard definition for green steel, the International Energy Agency (IEA) has suggested a quantitative benchmark for near-zero emissions steel production. Specifically, they propose a near-zero carbon-equivalent emission threshold of 0.4 tCO_2e/tLS for entirely ore-based steelmaking, decreasing linearly to 0.05 tCO_2e/tLS for steel produced solely from scrap [65]. For our scrap input of 212 kg/tLS, this yields a reference threshold of 0.33 tCO_2e/tLS. Note that the IEA's balance envelope includes selected Scope 3 emissions, i.e., from fossil fuel supply and lime flux production, whereas the present study adopts a gate-to-gate approach. Therefore, the indicated threshold is used here as a qualitative reference, rather than a directly comparable quantitative benchmark.

3. Results and discussion

3.1. Direct reduction plant

To begin, we examine the energy consumption of the direct reduction plant and show how it is affected by different metallization degrees and DRI outlet temperatures. Since the direct reduction plant consumes energy only in the form of electricity, we refer to this metric as specific electricity consumption. For a DR-grade ore-fed, H_2-based DRP, it can be seen in Fig. 3.

On a DRP-level, the electric rotary kiln and the H_2 pre-heater have the largest contribution in terms of electricity consumption, followed by the compressors. In the rotary kiln, the iron ore feed is pre-heated from 60 °C to 500 °C. Pre-heating serves to remove moisture and set the temperature required for the pre-oxidation of Fe_3O_4 to Fe_2O_3 (see Section 2.1.3). DRI exits the CFB reactor at a variable temperature level from 625 °C to 840 °C. As the CFB system is adiabatic, the H_2 pre-heater supplies the rest of the reduction enthalpy. The contribution of the compressors comes mainly from the reductant recycle compressor. It is responsible to make up for the pressure drop experienced by the reductant stream on its way through the CFB system and heat exchangers.

The specific electricity consumption of the rotary kiln increases slightly with higher DRI metallization degree. As there is oxygen mass transfer from solid to gas phase upon reduction, producing the same DRI mass, but at higher metallization degree, requires more iron ore to be pre-heated inside the rotary kiln. Additionally, the electricity demand of the H_2 pre-heater increases considerably with higher DRI metallization degree. This behavior can be attributed to the higher chemical H_2 use and the definition of the effective stoichiometric excess, SN_{eff}, as a function of the DRI metallization degree (see Section 2.1.3). When the DRI metallization degree exceeds 70 %, a CFB cascade is foreseen to avoid excessively large reactor sizes (see Table 2). At the DRI metallization degrees of 70 % and 87 %, the introduction of an additional CFB unit to the system leads to a discrete increase in electricity demand. For the H_2 pre-heater, this behavior arises from increased heat losses through the CFB riser walls; for the H_2 recycle compressor, it is due to a higher pressure drop. While these discrete increases in electricity consumption are visible in Fig. 3, their quantitative effect is relatively minor.

In our approach, the DRP outlet temperature values are selected to align with the reduction kinetics measurements reported by Habermann [48]. From the lowest to the highest DRI metallization degree (65 % to 95 %), the specific electricity consumption of the DRP rises by 21 % at a DRP outlet temperature of 625 °C and by 24 % at 840 °C. If the DRP outlet temperature is raised, the inlet temperature of the reductant stream must also increase, as this stream supplies the required reduction enthalpy. Thus, there is a considerable increase in the H_2 pre-heater duty. Conversely, the rotary kiln is not affected, as its operation is de-coupled from the CFB system.

The DRP outlet temperature, reductant inlet temperature and stoichiometric excess, SN_{eff}, must be carefully balanced to achieve adiabatic operation in the CFB system. In this work, we opted to hold SN_{eff} primarily at 4.0, as described in Section 2.1.3. Thus, raising the DRP outlet temperatures requires higher reductant inlet temperatures to maintain the energy balance. However, as the higher-temperature reductant gas is dosed in strong excess together with fine ore particles inside the CFB, there is an increased risk of sticking and reactor defluidization. Moreover, reaching very high pre-heating temperatures in a H_2 atmosphere necessitates advanced heating element materials, leading to higher technical risk and equipment cost [66,67]. By keeping the outlet temperature of the reductant pre-heater at a constant value, the endothermic reduction enthalpy can be supplied by increasing SN_{eff}. Raising SN_{eff} leads to higher plant CapEx, since all equipment inside the gas recirculation loop, including the costly H_2-pre-heater and feed-effluent heat recuperator, have to be oversized. We refer to Supplementary Information SI6.1 for a detailed study of the economic impact of varying DRP outlet temperatures and SN_{eff}.

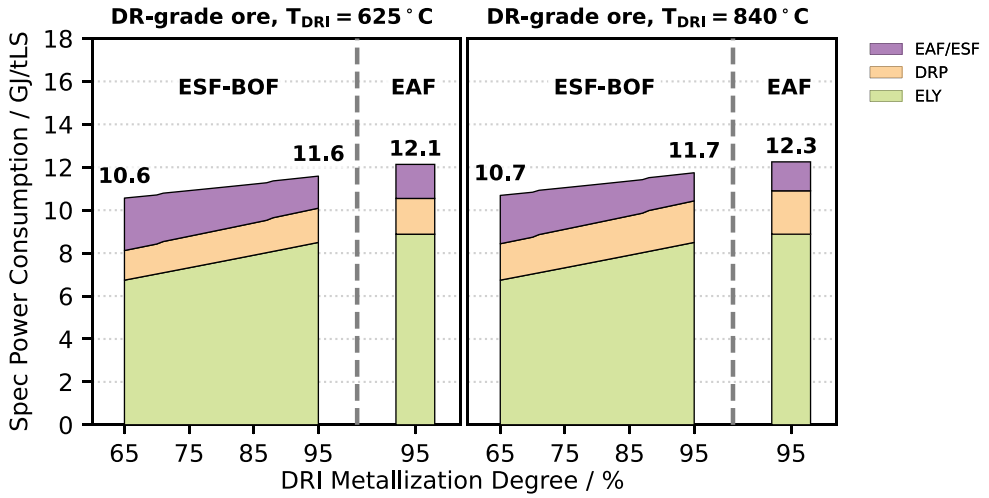

Fig. 4. Sensitivity analysis of the specific electricity consumption of the H_2DRI-ESF-BOF and H_2DRI-EAF routes against different DRP outlet temperatures and DRI metallization degrees for DR-grade ore. While the EAF is fed with DRI at a fixed metallization of 95 %, the ESF can process DRI charges with varying metallization degree. A temperature loss of 50 °C is considered between the DRP outlet and the EAF or ESF inlet. ELY: Pressurized-alkaline electrolysis; DRP: Direct reduction plant; EAF: Electric arc furnace; ESF: Electric smelting furnace.

3.2. Integrated steel production routes

3.2.1. Energy consumption

Further, we evaluate how the DRI metallization degree and outlet temperature affect the energy consumption of the integrated H_2DRI-EAF and H_2DRI-ESF-BOF process routes. As with the direct reduction plant, the integrated routes consume energy in the form of electricity only; therefore, their energy consumption is also quantified as specific electricity consumption. DR-grade ore is selected for illustration purposes in Fig. 4.

H_2 generation via electrolysis contributes the most to electricity use in both integrated steelmaking routes, followed by the DRP and steelmaking furnaces (EAF or ESF), depending on the DRP outlet temperature. In the H_2DRI-ESF-BOF route, reduction can be flexibly partitioned between the DRP and ESF. Increasing DRI metallization requires more green H_2 to the DRP, raising electricity input for both electrolyzer and DRP. Lower metallization shifts reduction to the ESF, increasing its electricity consumption, but decreasing that of the electrolyzer and DRP. Since the electrolyzer and DRP impacts dominate, specific electricity consumption rises with higher DRI metallization degrees. In this study, the stoichiometric excess, SN_{eff}, remains constant across the DRI metallization interval (see Section 2.1.3), but, especially at higher metallizations (e.g., after 87 %), SN_{eff} can be increased to enhance kinetics. The economic impact of adjusting SN_{eff} is discussed in Supplementary Information SI6.1.

As explained in Section 2.1.4, the EAF slag phase requires a fixed FeO content (25 %) to control the slag viscosity and enable its foaming behavior. Consequently, the more gangue present in DRI, the more iron is lost to the slag phase as FeO. In the ESF, modeled as a closed vessel with reducing atmosphere, considerably less FeO is formed and loss as slag component. Therefore, the specific electricity consumption of the H_2DRI-EAF route is higher than that of H_2DRI-ESF-BOF route even for the same, elevated DRI metallization degree of 95 %.

Varying the DRP outlet temperature reflects the counterbalancing effects of two factors: steelmaking and DRP electricity demand. It is evident that the steelmaking electricity demand decreases as the DRI charge temperature increases, since the gap between the feed-in temperature and the furnace operating temperature is reduced. In contrast, the electricity demand of the DRP increases, as previously explained in Section 3.1. All in all, varying the DRP outlet temperature had only limited effect on the specific electricity consumption of the overall system within the analyzed temperature range (625 °C to 840 °C).

3.2.2. Economics

The DRP outlet temperature had a low impact into the overall system's electricity use. Nevertheless, a lower DRP outlet temperature—though constrained by reaction kinetics—is expected to play an important role preventing sticking. Hence, we choose to fix it at 625 °C and compare the LCOS of the H_2DRI-EAF and H_2DRI-ESF-BOF routes with both DR-grade and BF-grade ores in Fig. 5.

Our results illustrate the superior robustness of the H_2DRI-ESF-BOF route against fluctuating iron ore purity, as opposed to the H_2DRI-EAF route. While replacing DR-grade by BF-grade ore results in a LCOS increase of 16 % for the H_2DRI-EAF route, the H_2DRI-ESF-BOF route experiences even a slight decline. When comparing the LCOS for BF-grade and DR-grade ore, it is important to recognize that the lower feedstock cost associated with BF-grade ore is counterbalanced by higher electricity consumption, increased demand for steelmaking fluxes, and greater CapEx requirements. The effects are both derived from a higher gangue content and a different gangue composition (ratio of SiO_2:MgO:CaO:Al_2O_3). In the case of the EAF, switching from DR-grade to BF-grade ore significantly increases the demand for fluxes, i.e., CaO and MgO (see Section 2.1.4), the CapEx of the steelmaking furnace and its electricity consumption. Even the lower cost of BF-grade ore is off-set by its higher material consumption, which results from the aforementioned Fe losses to the EAF slag phase. Compared to the H_2DRI-EAF route, the H_2DRI-ESF-BOF route is able to better capitalize on the lower iron ore cost: flux demand, i.e., CaO (see Section 2.1.4), furnace CapEx and electricity consumption of ESF do not increase meaningfully. Also, there is an additional revenue stream, by selling the larger amounts of ESF slag at a price level corresponding to granulated blast furnace slag.

On the topic of steelmaking furnace CapEx, we introduce a volumetric approach to evaluate the impact of different ore qualities on the CapEx of EAF and ESF. Note that the BOF's CapEx is independent of the ore composition, as gangue components are previously removed in the ESF. The relative volumetric differences in EAF and ESF batch volumes are illustrated in Fig. 6.

The results demonstrate that the higher EAF slag formation has indeed an enormous impact in terms of furnace volume. For the DR-grade ore, the EAF slag occupies 70 % of the volume of liquid steel phase. Meanwhile, the ESF slag takes up merely 40 % of the volume of the hot metal phase. For the BF-grade feedstock, the EAF slag phase has for more than double the volume of the liquid steel phase. Meanwhile, the ESF slag possesses roughly 10 % more volume compared to the hot

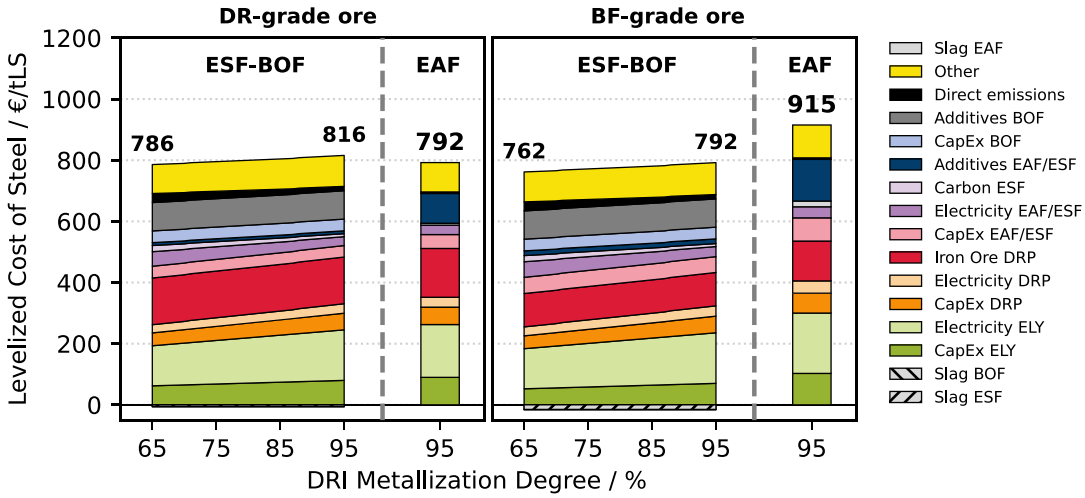

Fig. 5. Levelized cost of steel resulting from H_2DRI-EAF and H_2DRI-ESF-BOF routes, respectively, starting from DR-grade and BF-grade ores and DRP outlet temperature of 625 °C. While the EAF is fed with DRI at a fixed metallization degree of 95 %, the ESF can process DRI charges with varying metallization degree. A temperature loss of 50 °C is considered between the DRP outlet and the EAF or ESF inlet. ELY: Pressurized-alkaline electrolysis; DRP: Direct reduction plant; EAF: Electric arc furnace; ESF: Electric smelting furnace; BOF: Basic oxygen furnace; Additives EAF/ESF/BOF: Residual input materials necessary to fulfill the specifications detailed in Section 2.1.4.

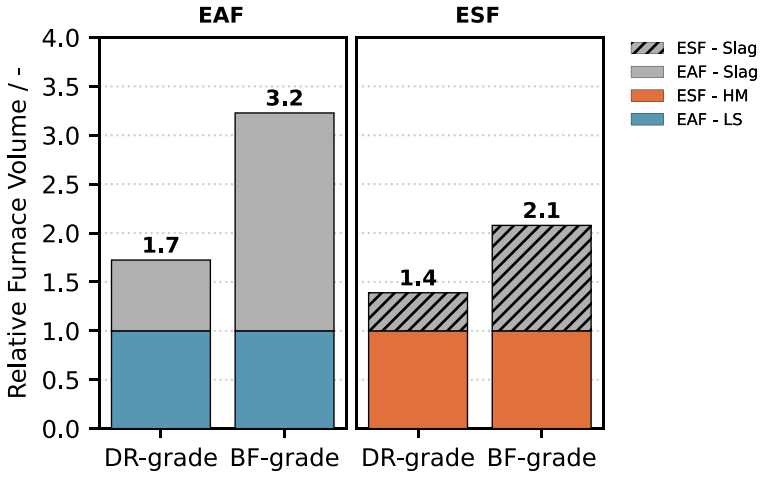

Fig. 6. Relative volumes of electric arc furnace (EAF) (left) and electric smelting furnace (ESF) (right) charged with DRI from DR-grade and BF-grade ores. Note: In the EAF, scrap metal is charged alongside DRI as low-cost and low-GHG iron source to improve its overall comparability with the ESF-BOF route. In contrast, the ESF is fed purely with DRI as iron source, with scrap metal being introduced subsequently in the BOF. Feeding the EAF with DRI only would further increase its volumetric ratio of slag to liquid steel. HM: hot metal; LS: liquid steel.

metal phase. While the ESF slag is potentially able to find off-takers in the cement industry, there is very limited use for the EAF slag. Thus, the EAF slag brings about a double penalty: higher steelmaking CapEx and slag disposal costs. From a technical perspective, operating an EAF with such large slag volumes might bring about additional challenges of technical nature.

In Fig. 5, comparing the H_2DRI-ESF-BOF route with BF-grade ore against the H_2DRI-EAF route with DR-grade ore, there are certain aspects to bear in mind. The LCOS achieved through both routes is quite similar. Although our approach considers volumetric differences, we still rely on an estimated specific ESF CapEx at a reference state, as described in Section 2.2.1. Moreover, our simplified iron ore costing approach results in a levelized cost of iron ore increase of 60 % between BF-grade and DR-grade feedstock (75 €/t versus 120 €/t). While this may hold for a vertically integrated complex, assuming ore beneficiation to a flexible level inside the battery limits is technically feasible, projects relying on external iron ore sourcing are expected to experience even more pronounced price premiums for DR-grade feedstock. For reference, from 2006 to 2016, the weighted average Fe content of iron ore supplied by the so-called *Big Four* miners (Vale, Rio Tinto, BHP and Fortescue) shrank from 62 % to 61 % [34]. As the ore quality further deteriorates, the price gap between lower-grade and DR-grade ores is expected to grow. Growing price gaps would make the H_2DRI-ESF-BOF route even more attractive compared to the H_2DRI-EAF route.

To further assess the economics of both processes, it is imperative determine how resilient they are against fluctuating market conditions. As the H_2DRI-EAF route clearly underperforms when processing lower-grade feed, we take its operation based on DR-grade feedstock as benchmark. As for the H_2DRI-ESF-BOF route, BF-grade feedstock is chosen to unlock access to a larger share of the iron ore export market. Here, we analyze the sensitivity of both routes' LCOS with respect to electricity prices, as seen in Fig. 7.

Because H_2 generation, direct reduction, and steelmaking are powered by electricity, the associated electricity price predominantly determines their operating expenses and thus plays a crucial role in green steel economics. For the H_2DRI–EAF route, a fivefold increase in electricity price (from 30 €/MWh to 150 €/MWh) results in a 62 %

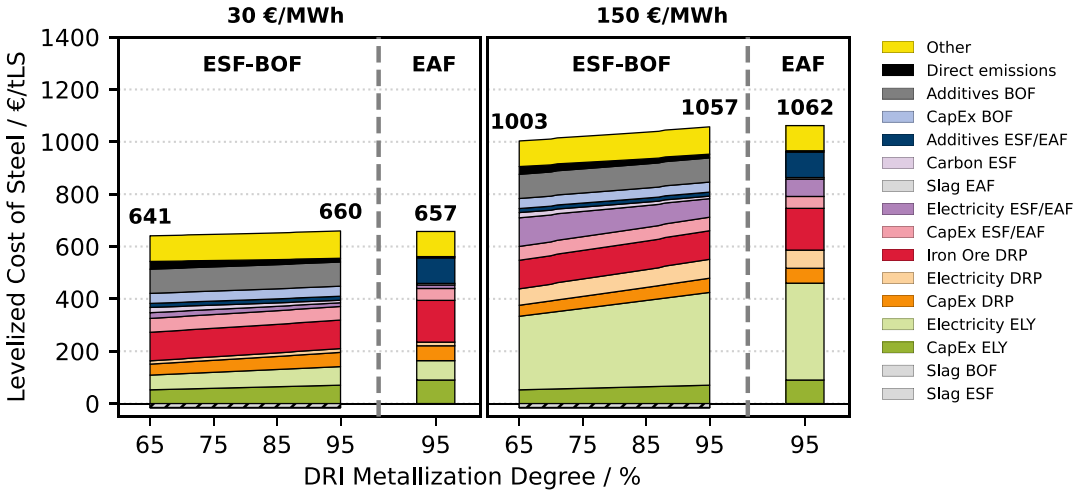

Fig. 7. Sensitivity analysis of the levelized cost of steel resulting from H_2DRI-EAF (with DR-grade ore) and H_2DRI-ESF-BOF (with BF-grade ore) routes against the electricity price. While the EAF is fed with DRI from DR-grade ore at a fixed metallization degree of 95 %, the ESF is fed with DRI from BF-grade ore with varying metallization degrees. A temperature loss of 50 °C is considered between the DRP outlet and the EAF or ESF inlet. ELY: Pressurized-alkaline electrolysis; DRP: Direct reduction plant; EAF: Electric arc furnace; ESF: Electric smelting furnace; BOF: Basic oxygen furnace; Additives EAF/ESF/BOF: Residual input materials necessary to fulfill the specifications detailed in Section 2.1.4.

rise in LCOS. The H_2DRI–ESF–BOF configuration offers a slight mitigation of this sensitivity by lowering the DRI metallization degree. At a metallization degree of 65 %—the lowest value examined for this route—the same fivefold increase in electricity price leads to a 56 % increase in LCOS. However, reducing the DRI metallization degree directly raises the GHG emissions of the produced steel, as H_2 reductant is increasingly substituted by carbon. The interested reader will find an additional sensitivity analysis of LCOS with respect to scrap price in Supplementary Information SI6.2.

3.2.3. Greenhouse gas emissions

The impact of electricity is not restricted to economics. Due to the high electricity consumption, the GHG emissions for production of green steel (see Section 2.2.2) are largely determined by the GHG intensity of the respective electricity source. We compare the specific GHG emissions of the H_2DRI-EAF and H_2DRI-ESF-BOF routes in Fig. 8.

Direct emissions of the H_2DRI-EAF route originate from carbon input that is required only to reach the desired carbon content in steel. Hence, the contribution of direct emissions in this route is very limited. For a defined steel quality (i.e., mild steel with same C content), it does not vary with respect to the iron ore source. When fully powered by renewable energy, the EAF-based route has the potential to bring GHG emissions to near-zero (0.06 tCO_2e/tLS). To reach this value, an integrated H_2DRI-EAF facility running for 8000 h per year would require a total of ca. 1.1 GW of installed renewable power for a typical plant capacity of 2.5 mtpa liquid steel (without accounting for renewable energy utilization factors, energy conversion and transmission losses). The massive electricity demand constitutes a significant challenge from a commercial perspective, involving the securing of sufficient, long-term renewable power purchase agreements. From an infrastructure standpoint, massive expansion of renewable energy sources, grid-scale storage, and sufficient grid access are required to sustain steady-state operation for 8000 h per year. Alternatively, direct coupling of intermittent renewable power to the steel production plant necessitates over-dimensioned renewable generation and electrolyzer capacity alongside battery and hydrogen storage systems. At renewable energy utilization factors of 50 % to 30 %, the required installed renewable power ranges from 2.1 GW to 3.5 GW.

The non-binding, IEA-proposed threshold for green steel, introduced in Section 2.2.2, depends on the scrap feed rate and lies at 0.33 tCO_2e/tLS in our case. With its very low direct emissions, the H_2DRI-EAF route still has the potential to comply with this threshold. We are not able to calculate the highest electricity-related GHG intensity that still complies with such threshold, as our GHG balance envelope does not include certain Scope 3 emissions (from fossil fuel supply and lime flux production) that are included in their definition (see Section 2.2.2).

As opposed to the direct emissions, the Scope 2 emissions of the H_2DRI-EAF route are affected by the iron ore purity. There is a 16 % increase in GHG emissions when switching from DR-grade to BF-grade feedstock, caused by three main factors. Firstly, there is a higher specific H_2 consumption, as more of the direct reduced iron is loss to the slag phase, in order to reach the intrinsic FeO content necessary for EAF operation. Furthermore, the specific electricity consumption in both the DRP and EAF increase with more gangue, respectively, absorbing heat and being molten inside these units. In our worst-case scenario, the electricity mix has a GHG intensity 600 gCO_2e/kWh. Under such circumstance, there will be no significant GHG savings compared to the average BF-BOF route with 2.32 tCO_2/tCS [68].

As for the H_2DRI-ESF-BOF route, its direct emissions originate from the carbon input that is required to both reduce the remaining oxidized iron species and carburize the hot metal. Owing to the former, its contribution decreases with increasing DRI metallization degree. When fully supplied with renewable electricity, the ESF route attains a minimum GHG emissions level of 0.18 tCO_2e/tLS at the highest DRI metallization degree of 95 %, rising linearly to 0.37 tCO_2e/tLS at the lowest DRI metallization of 65 %. Even at high DRI metallization degrees, compliance with the aforementioned IEA-proposed threshold (see Section 2.2.2) without CO_2 capture appears challenging, as we do not account for any Scope 3 emissions in our framework. It is important to mention that this threshold has not yet been adopted by any official regulating bodies. We discuss certain process measures to facilitate compliance with this threshold in Sections 4 and 4.

Analogous to the direct emissions, Scope 2 emissions associated with electricity consumption in the ESF decrease as the metallization degree of the DRI charge increases. These effects are counterbalanced by the remaining Scope 2 emissions, originating from electricity demand in the DRP and H_2 production unit. Following the electricity consumption trend, the GHG emissions of H_2DRI-ESF-BOF are also more robust against decreasing feedstock purity. They increased only by 2 % to 3 % switching from DR-grade to BF-grade feedstock.

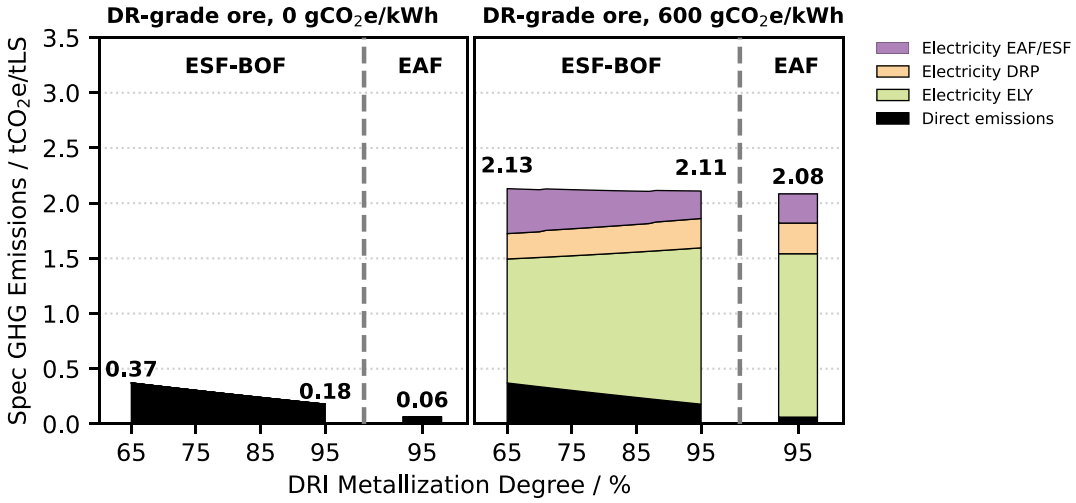

(a) Specific GHG emissions of H_2DRI-EAF and H_2DRI-ESF-BOF routes fed with DR-grade ore, based on electricity-related GHG intensities of 0 gCO_2e/kWh (left) and 600 gCO_2e/kWh (right).

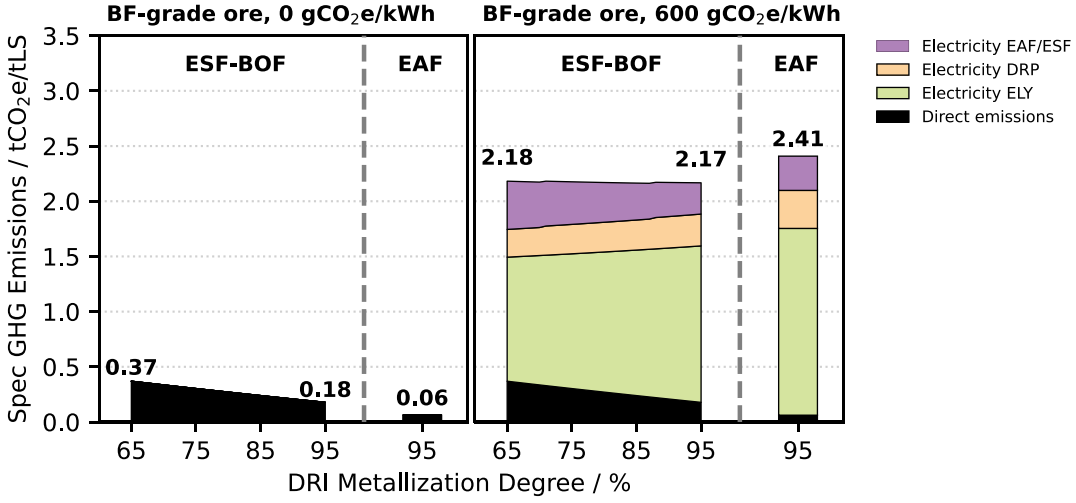

(b) Specific GHG emissions of H_2DRI-EAF and H_2DRI-ESF-BOF fed with BF-grade ore, based on electricity-related GHG intensities of 0 gCO_2e/kWh (left) and 600 gCO_2e/kWh (right).

Fig. 8. Sensitivity analysis of the Scope 1 (direct) and 2 (indirect, energy-related) specific GHG emissions for the H_2DRI-EAF and H_2DRI-ESF-BOF routes against the electricity-related GHG intensity. Direct emissions: ESF and BOF off-gases; ELY: Pressurized-alkaline electrolysis; DRP: Direct reduction plant; EAF: Electric arc furnace.

3.2.4. *Trade-offs between economics and greenhouse gas emissions*

By comparing Figs. 5 and 8, it becomes evident that, under our base-case assumptions, the LCOS decreases with increasing GHG intensity for steel produced via the H_2DRI-ESF-BOF route. This trend is largely driven by the assumed low GHG emission penalty of 80 €/tCO_2 and the calculated high levelized cost of H_2 (LCOH) of 6.4 €/kgH_2. These values represent a realistic, yet short-term scenario for countries without strict GHG regulations or widespread access to low-cost renewables. GHG emission penalties are expected to increase continuously to provide incentives for adopting sustainable technologies. In addition, the LCOH strongly correlates with the cost of electricity, meaning that in some geographies with abundant and affordable clean energy, lower values can already be achieved today or within few years. Also, the CapEx of green H_2 plants is projected to undergo significant reductions as H_2 demand grows and electrolyzer technologies mature further [69]. Fig. 9 presents a bi-level analysis of the LCOS as a function of GHG emissions for the H_2DRI-ESF-BOF route (based on BF-grade ore), with varying GHG emission penalties and LCOH values. Each parameter is varied independently, while the other one is held at its short-term value. A complementary trade-off diagram, in which each parameter is varied, while the other one is held at its future-term value, is provided in Supplementary Information SI6.3.

Up to a GHG emission penalty of 190 €/tCO_2e, we observe a linear decrease in LCOS with higher GHG emissions. From this value onwards, this trend is reversed, so that it makes economically more sense to reduce the GHG emissions of the produced steel. In spite of this qualitative trend, increasing the GHG emission penalty has a relatively limited impact on the overall LCOS value. While it might serve as a bridging tool to align economics with GHG emissions, it does not provide meaningful incentives for GHG mitigation inside the H_2DRI-ESF-BOF route.

The LCOH has a much more decisive impact on the LCOS, reflected by the greater variance in LCOS upon variations of the LCOH compared to the applied GHG emission penalty. We find that around 3.9 €/kgH_2 there is an even trade-off between LCOS and GHG emissions along the DRI metallization degree interval. Higher LCOH values create an economic incentive to lower the DRI metallization degree, which increases specific GHG emissions; conversely, at lower LCOH values,

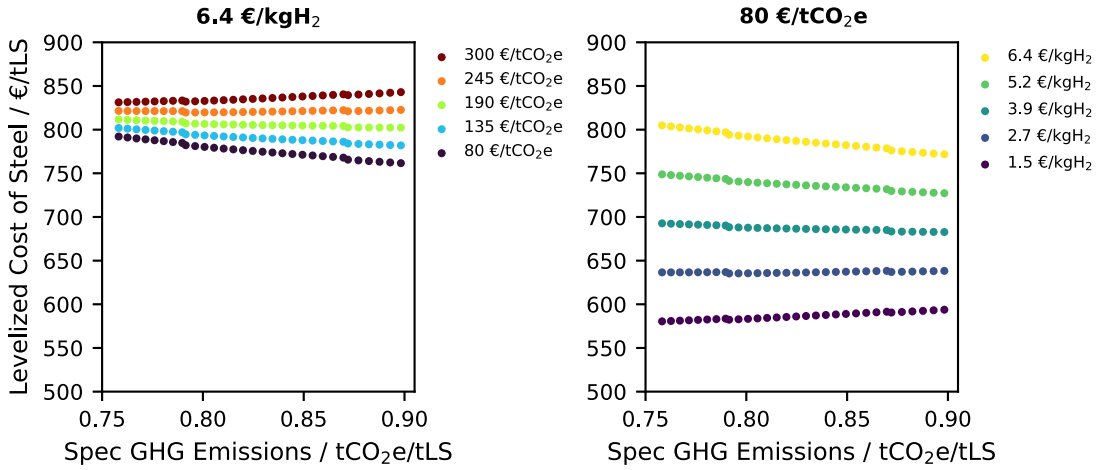

Fig. 9. Sensitivity analysis of the levelized cost of steel versus Scope 1 (direct) and 2 (indirect, energy-related) specific GHG emissions for the H_2DRI-ESF-BOF route fed with BF-grade ore against different GHG emission penalties and levelized costs of H_2 (LCOH). On the left, the LCOH is kept constant at 6.4 €/kgH_2; on the right, the GHG penalty is kept constant at 80 €/tCO_2e. In both cases, the electricity-related GHG intensity of 175 gCO_2e/kWh is applied as forecast for the European grid in 2025 [70].

steel with lowest GHG emissions offers the lowest cost. At the lowest LCOH of 1.5 €/kgH_2, which requires drastic CapEx reductions and a very competitive electricity price, LCOS values range from 565 €/tLS to 578 €/tLS depending on the DRI metallization degree. For reference, after undergoing secondary metallurgy, crude steel is largely traded in the global markets, e.g., as hot-rolled coil (HRC), with an average market price from 445 €/tHRC to 544 €/tHRC [71]. The current low prices demonstrate the immense commercial pressure faced by decarbonized steel products.

4. Conclusions

In this study, we compare the performance of H_2DRI-EAF and H_2DRI-ESF-BOF routes for processing (magnetitic) low-grade and high-grade iron ore fines into steel. By integrating a process simulation of the H_2-based, CFB direct reduction with a metallurgical thermodynamic analysis of the steelmaking furnaces, we investigate how variations in ore quality and the distribution of reduction between CFB and ESF units affect overall electricity consumption, levelized cost of steel and specific GHG emissions of these routes.

On a DRP-level, the DRI metallization degree and DRP outlet temperature have a considerable impact on the electricity consumption. Taking a look into the overall process routes, the impact of the DRP outlet temperature becomes negligible, as it just shifts electricity consumption between the direct reduction and the steelmaking plants inside the analyzed temperature interval. The DRI metallization degree still has a noticeable impact on the electricity consumption of the H_2DRI-ESF-BOF route.

Reducing the DRI metallization degree plays a moderate (yet positive) role in levelized cost for the H_2DRI-ESF-BOF route. We show this effect may become more pronounced if the stoichiometric excess, SN_{eff} has to be raised to achieve higher DRI metallization degree. Altogether, it makes a strong point for operating the ESF in combination with H_2-based CFB reduction of fine ore, as the latter might not even be able to reach high DRI metallization due to increased sticking. Regarding ore quality, the H_2DRI-EAF route shows strong sensitivity, resulting from higher electricity consumption, Fe losses, and steelmaking furnace CapEx. Note that we assess steel furnace economics based on thermodynamic behavior; in practice, operating an EAF with enormous slag formation from low-grade ore may not be feasible. For reference, slag—due to lower density—occupies 120 % of liquid steel volume in an EAF batch with low-grade ore.

Conversely, the H_2DRI-ESF-BOF route is able to effectively capitalize on the lower cost of low-purity iron ore feedstock. Its steelmaking electricity consumption and steelmaking batch volume are robust against lower ore qualities, with its slag phase generating additional revenue off-setting clinker demand for cement production.

We find that electricity costs are a key lever for achieving competitive green steel economics—especially in vertically integrated complexes, where electrolysis, direct reduction and steelmaking are large electricity consumers. The H_2DRI-EAF route's sensitivity against electricity prices is slightly higher than that of the H_2DRI-ESF-BOF route. Beyond economics, supplying electricity to such large-scale, integrated green steel facilities may become a bottleneck from an infrastructure standpoint.

The electricity-related GHG intensity has a large contribution on the specific GHG emissions of the produced steel. While iron ore quality plays a decisive role on the GHG emissions in the H_2DRI-EAF route, this does not materialize for the H_2DRI-ESF-BOF route. Benchmarking the direct emissions calculated in this work against the non-binding, IEA-proposed GHG emission threshold for green steel reveals that the H_2DRI-EAF route is more likely to comply. For the H_2DRI-ESF-BOF route, a high DRI metallization degree would be desired. Lower carburization of the hot metal would decrease direct emissions of this route, albeit having a far-reaching metallurgical impact (limited nitrogen removal), which has to be further investigated. Capturing CO_2 from the ESF offgas and or (partially) substituting fossil carbon by biochar represent additional measures to facilitate compliance with GHG emission thresholds.

Analyzing the trade-offs between economics and GHG emissions for the H_2DRI-ESF-BOF route, we find that GHG emission penalties can provide a certain incentive to minimize GHG emissions. However, its impact on the overall LCOS values is rather limited. Our results underpinned, however, the overwhelming contribution of H_2 reductant supply on the economics of green steel via the H_2DRI-ESF-BOF route. This creates risks for regions lacking abundant, cheap renewables. Decoupling H_2 production and ironmaking from integrated steelmaking—by importing chemical H_2 carriers [72] or hot-briquetted iron [73]—can help less-resourced countries retain a stake in steel manufacturing. Additionally, this approach can relieve infrastructure constraints and unlock new opportunities for heat integration. Segregated, geography-optimized value chains for the H_2DRI-EAF route have been discussed [74], yet many avenues remain unexplored: only NH_3 is contemplated as chemical H_2 carrier, and synergies between NH_3 cracking and direct reduction are still to be investigated on a

flowsheet level. Future studies should encompass the material and heat integration between direct reduction and the H_2 reconversion from different chemical H_2 carriers (ammonia, methanol, dimethyl ether, liquid organic hydrogen carriers). Advancing these solutions will help unlock the full promise of green steel as a key pillar in a sustainable, hydrogen-based economy.

CRediT authorship contribution statement

João Miguel Margutti: Writing – original draft, Writing – review & editing, Methodology, Investigation, Conceptualization. **Matthias Schiedeck:** Writing – review & editing, Methodology, Investigation, Conceptualization. **Philipp Morsch:** Writing – review & editing, Supervision, Methodology, Conceptualization. **Sarah Deutz:** Supervision, Writing – review & editing. **Sabrine Khadhraoui:** Methodology, Investigation. **Thomas Wolfinger:** Methodology, Investigation. **Andreas Peschel:** Writing – review & editing, Supervision, Conceptualization.

Declaration of generative AI and AI-assisted technologies in the manuscript preparation process

During the preparation of this work the authors used Perplexity AI in order to improve readability and grammatical correctness of the manuscript. After using this tool, the authors reviewed and edited the content as needed and take full responsibility for the content of the published article.

Declaration of competing interest

The authors declare that they have no known competing financial interests or personal relationships that could have appeared to influence the work reported in this paper.

Acknowledgments

The authors acknowledge the funding by the German Federal Ministry of Research, Technology and Space (BMFTR) (under grant number 03SF0746A). Further, we are grateful to Dr. Elena Yazhenskikh and PD Dr. Michael Müller at the institute IMD-1 of Forschungszentrum Jülich for enabling access to their institute's virtual infrastructure and their initial support with metallurgical thermodynamics. Finally, we thank Clarissa Reisen and Markus Hübner for the graphical support.

Appendix A. Supplementary data

Supplementary material related to this article can be found online at https://doi.org/10.1016/j.ijhydene.2026.155073.

References

[1] World Steel Association. World steel in figures 2025. Technical report, 2025, URL: https://worldsteel.org/data/world-steel-in-figures/world-steel-in-figures-2025/.

[2] Friedlingstein P, O'Sullivan M, Jones MW, Andrew RM, Hauck J, Landschützer P, Le Quéré C, Li H, Luijkx IT, Olsen A, Peters GP, Peters W, Pongratz J, Schwingshackl C, Sitch S, Canadell JG, Ciais P, Jackson RB, Alin SR, Arneth A, Arora V, Bates NR, Becker M, Bellouin N, Berghoff CF, Bittig HC, Bopp L, Cadule P, Campbell K, Chamberlain MA, Chandra N, Chevallier F, Chini LP, Colligan T, Decayeux J, Djeutchouang LM, Dou X, Duran Rojas C, Enyo K, Evans W, Fay AR, Feely RA, Ford DJ, Foster A, Gasser T, Gehlen M, Gkritzalis T, Grassi G, Gregor L, Gruber N, Gürses Ö, Harris I, Hefner M, Heinke J, Hurtt GC, Iida Y, Ilyina T, Jacobson AR, Jain AK, Jarníková T, Jersild A, Jiang F, Jin Z, Kato E, Keeling RF, Klein Goldewijk K, Knauer J, Korsbakken JI, Lan X, Lauvset SK, Lefèvre N, Liu Z, Liu J, Ma L, Maksyutov S, Marland G, Mayot N, McGuire PC, Metzl N, Monacci NM, Morgan EJ, Nakaoka S-I, Neill C, Niwa Y, Nützel T, Olivier L, Ono T, Palmer PI, Pierrot D, Qin Z, Resplandy L, Roobaert A, Rosan TM, Rödenbeck C, Schwinger J, Smallman TL, Smith SM, Sospedra-Alfonso R, Steinhoff T, Sun Q, Sutton AJ, Séférian R, Takao S, Tatebe H, Tian H, Tilbrook B, Torres O, Tourigny E, Tsujino H, Tubiello F, van der Werf G, Wanninkhof R, Wang X, Yang D, Yang X, Yu Z, Yuan W, Yue X, Zaehle S, Zeng N, Zeng J. Global carbon budget 2024. Earth Syst Sci Data 2025;17(3):965–1039. http://dx.doi.org/10.5194/essd-17-965-2025.

[3] Cardoso W, Felice RD. Forecast of carbon consumption of a blast furnace using extreme learning machine and probabilistic reasoning. Chem Eng Trans 2022;96:493–8. http://dx.doi.org/10.3303/CET2296083, URL: https://www.cetjournal.it/index.php/cet/article/view/12930.

[4] Król A. The role of the granulated blast furnace slag in sustainable cement production and waste management. Econ Environ Stud 2017;17(43):613–24. http://dx.doi.org/10.25167/ees.2017.43.10.

[5] World Steel Association. Sustainability performance of the steel industry. Sustain Indic Rep 2025 2025. URL: https://worldsteel.org/wider-sustainability/sustainability-indicators/.

[6] Johnson C, Åhman M, Nilsson LJ, Li Z. Emerging green steel markets surrounding the EU emissions trading system and carbon border adjustment mechanism. Nat Commun 2025;16(1):9087. http://dx.doi.org/10.1038/s41467-025-64440-9.

[7] Sarkar S, Bhattacharya R, Roy GG, Sen PK. Modeling MIDREX based process configurations for energy and emission analysis. Steel Res Int 2018;89(2). http://dx.doi.org/10.1002/srin.201700248.

[8] Fennell P, Driver J, Bataille C, Davis SJ. Cement and steel - nine steps to net zero. Nature 2022;603(7902):574–7. http://dx.doi.org/10.1038/d41586-022-00758-4.

[9] Soroush Basirat. Hydrogen unleashed: Opportunities and challenges in the evolving H2-DRI-EAF pathway beyond 2024. Technical report, 2025, URL: https://ieefa.org/resources/hydrogen-unleashed-opportunities-and-challenges-evolving-h2-dri-eaf-pathway-beyond-2024.

[10] Wang RR, Zhao YQ, Babich A, Senk D, Fan XY. Hydrogen direct reduction (h-DR) in steel industry—An overview of challenges and opportunities. J Clean Prod 2021;329:129797. http://dx.doi.org/10.1016/j.jclepro.2021.129797.

[11] Lopes DV, Quina MJ, Frade JR, Kovalevsky AV. Prospects and challenges of the electrochemical reduction of iron oxides in alkaline media for steel production. Front Mater 2022;9. http://dx.doi.org/10.3389/fmats.2022.1010156.

[12] Draxler M, Sormann A, Kempken T, Hauck T, Pierret JC, Borlee J, Di Donato A, de Santis M, Wang C. Technology assessment and roadmapping (deliverable 1.2). Technical report, Green Steel for Europe Consortium: Brussels, Belgium; 2021, URL: https://www.estep.eu/assets/projects/greensteel4europe/greensteel_publication/210308_d1-2_-assessment_and_roadmapping_of_technologies_-publishable-version.pdf.

[13] Souza Filho IR, Springer H, Ma Y, Mahajan A, Da Silva CC, Kulse M, Raabe D. Green steel at its crossroads: Hybrid hydrogen-based reduction of iron ores. J Clean Prod 2022;340:130805. http://dx.doi.org/10.1016/j.jclepro.2022.130805.

[14] Jovičević-Klug M, Souza Filho IR, Springer H, Adam C, Raabe D. Green steel from red mud through climate-neutral hydrogen plasma reduction. Nature 2024;625(7996):703–9. http://dx.doi.org/10.1038/s41586-023-06901-z.

[15] Vogl V, Åhman M, Nilsson LJ. Assessment of hydrogen direct reduction for fossil-free steelmaking. J Clean Prod 2018;203:736–45. http://dx.doi.org/10.1016/j.jclepro.2018.08.279.

[16] Müller N, Herz G, Reichelt E, Jahn M, Michaelis A. Assessment of fossil-free steelmaking based on direct reduction applying high-temperature electrolysis. Clean Eng Technol 2021;4:100158. http://dx.doi.org/10.1016/j.clet.2021.100158.

[17] Jacobasch E, Herz G, Rix C, Müller N, Reichelt E, Jahn M, Michaelis A. Economic evaluation of low-carbon steelmaking via coupling of electrolysis and direct reduction. J Clean Prod 2021;328:129502. http://dx.doi.org/10.1016/j.jclepro.2021.129502.

[18] Rosner F, Papadias D, Brooks K, Yoro K, Ahluwalia R, Autrey T, Breunig H. Green steel: design and cost analysis of hydrogen-based direct iron reduction. Energy Environ Sci 2023;16(10):4121–34. http://dx.doi.org/10.1039/D3EE01077E.

[19] Scaccabarozzi R, Artini C, Mastropasqua L, Mapelli C, Brouwer J, Kim JY, Ghezel-Ayagh H, Lehman P, Jampani M, Cavlovich N, Campanari S, Romano MC, Spinelli M. Technical analysis of high-efficiency and flexible direct reduced iron plants integrated with high-temperature electrolysis. J Clean Prod 2025;489:144681. http://dx.doi.org/10.1016/j.jclepro.2025.144681.

[20] Immonen J, Weingaertner D, Ketkaew J, Prasher R, Powell KM. Process intensification and comparison of electrolytic hydrogen green steel plants for industrial decarbonization. J Clean Prod 2025;490:144812. http://dx.doi.org/10.1016/j.jclepro.2025.144812.

[21] Manning C, Chevrier VF. Maximizing iron unit yield from ore to liquid steel (part 1 – ore selection). Technical report, 2019, URL: https://www.midrex.com/tech-article/maximizing-iron-unit-yield-from-ore-to-liquid-steel-part-1-ore-selection/.

[22] Wilmoth R, Homann Q, Gamage C, Wright L, Ramirez K, Flesch S, Ha T, Rosas J, Janzow N. Green iron corridors: Transforming steel supply chains for a sustainable future. Technical report, RMI; 2024, URL: https://rmi.org/insight/green-iron-corridors-transforming-steel-supply-chains-for-a-sustainable-future/.

[23] Lovón-Canchumani GA, Lima FMS, Araujo MG, Elabras-Veiga LB. Environmental impacts for iron ore pellet production: A study of an open pit mine through life cycle assessment. Sci Total Environ 2025;993:179986. http://dx.doi.org/10.1016/j.scitotenv.2025.179986.

[24] Spreitzer D, Schenk J. Fluidization behavior and reducibility of iron ore fines during hydrogen-induced fluidized bed reduction. Particuology 2020;52:36–46. http://dx.doi.org/10.1016/j.partic.2019.11.006.

[25] Wolfinger T, Spreitzer D, Schenk J. Analysis of the usability of iron ore ultrafines for hydrogen-based fluidized bed direct reduction-a review. Mater (Basel, Switzerland) 2022;15(7). http://dx.doi.org/10.3390/ma15072687.

[26] Zhang J, Li S, Wang L. Kinetics analysis of direct reduction of iron ore by hydrogen in fluidized bed based on response surface methodology. 49, 2024, p. 1318–31. http://dx.doi.org/10.1016/j.ijhydene.2023.09.243, 0360-3199.
[27] Parvathaneni S, Kodukula B, Andrade MW. Iron-ore reduction in fluidized beds: Review of commercial technologies, status, and challenges. Ind Eng Chem Res 2024;63(44):18724–33. http://dx.doi.org/10.1021/acs.iecr.4c02282.
[28] Elmquist S. Operational results of the Circored fine ore direct reduction plant in Trinidad. Technical Report, 2002.
[29] Mesquita J, Badawi M, Belissont R, Turrer H, Foucaud Y. Assessment of flotation process efficiency in producing DR concentrate from a low-grade iron ore. Miner Eng 2024;216:108838. http://dx.doi.org/10.1016/j.mineng.2024.108838.
[30] Fruehan RJ. The making, shaping and treating of steel: Steelmaking volume. Technical report, Pittsburgh, PA: AISE Steel Foundation; 1998.
[31] von Schéele J. Pathways towards full use of hydrogen as reductant and fuel. Matériaux Tech 2023;111(4):405. http://dx.doi.org/10.1051/mattech/2023030.
[32] Kim W, Sohn I. Critical challenges facing low carbon steelmaking technology using hydrogen direct reduced iron. Joule 2022;6(10):2228–32. http://dx.doi.org/10.1016/j.joule.2022.08.010.
[33] Aminorroaya-Yamini S, Edris H. The effect of foamy slag in electric arc furnaces on electric energy consumption. Technical report, 2002, URL: https://ro.uow.edu.au/articles/conference_contribution/the_effect_of_foamy_slag_in_electric_arc_furnaces_on_electric_energy_consumption/27693120.
[34] S. Nicholas SB. Iron ore quality a potential headwind to green steelmaking. Technical report, 2022, URL: https://ieefa.org/sites/default/files/2022-06/iron%20ore%20quality%20a%20potential%20headwind%20to%20green%20steelmaking_june%202022.pdf.
[35] Dong XF, Longbottom R, Guo BY, Monaghan B, Zulli P. Transitional path to low-carbon steel production: A review of current pathways and modeling of the electric smelting furnace process. J Sustain Met 2025. http://dx.doi.org/10.1007/s40831-025-01292-z.
[36] Yang C, Wei L, Zhu D, Pan J, Xia G, Qu S. Hydrogen-based direct reduction behavior of iron ore pellets with iron grades ranging from 59 % to 68 %. 138, 2025, p. 787–801. http://dx.doi.org/10.1016/j.ijhydene.2025.04.006, 0360-3199.
[37] Garlick C, Singh T, Paymooni K, O'Dea D, Honeyands T. Electrode smelting of hydrogen-reduced Hematite–Goethite at laboratory scale. J Sustain Met 2025. http://dx.doi.org/10.1007/s40831-025-01281-2.
[38] Wimmer G, Voraberger B, Rosner J, Pfeiffer A. Smelter - green steelmaking using low-grade DRI. Iron Steel Technol 2025.
[39] Geldenhuys I, Terblanche G, Louw S. Advancing electric smelting for sustainable iron production: Pilot-scale validation of controlled open-arc DC technology. Iron Steel Technol 2026. URL: https://www.aist.org/getmedia/be583fc6-ed6f-490f-aa31-df4596bb6526/January-2026_050-060.pdf.
[40] Rahbari A, Shahabuddin M, Sabah S, Brooks G, Pye J. Production of green steel from low-grade ores: An end-to-end techno-economic assessment. Cell Rep Sustain 2025;2(1):100301. http://dx.doi.org/10.1016/j.crsus.2024.100301.
[41] Gerloff N. Comparative life-cycle-assessment analysis of three major water electrolysis technologies while applying various energy scenarios for a greener hydrogen production. J Energy Storage 2021;43:102759. http://dx.doi.org/10.1016/j.est.2021.102759.
[42] Kim W-H, Lee S, Kim S-M, Min D-J. The retardation kinetics of magnetite reduction using H2 and H2–H2O mixtures. Int J Hydrog Energy 2013;38(10):4194–200. http://dx.doi.org/10.1016/j.ijhydene.2013.01.147.
[43] Lorente E, Herguido J, Peña JA. Steam-iron process: Influence of steam on the kinetics of iron oxide reduction. Int J Hydrog Energy 2011;36(21):13425–34. http://dx.doi.org/10.1016/j.ijhydene.2011.07.111.
[44] Steffen R, Tacke K-H, Pluschkell W. Grundlagenuntersuchungen zur umweltfreundlichen Reduktion von Eisenerz mit Wasserstoff oder wasserstoffreichen Gemischen. Technical report, 1998.
[45] Pichler A, Mali H, Plaul F, Schenk J, Skorianz M, Weiss B. Reduction behavior and structural evolution of iron ores in fluidized bed technologies—Part 2: Characterization and evaluation of worldwide traded fine iron ore brands. Steel Res Int 2016;87(5):642–52. http://dx.doi.org/10.1002/srin.201500176.
[46] Thurnhofer A, Schachinger M, Winter F, Mali H, Schenk JL. Iron ore reduction in a laboratory-scale fluidized bed reactor-effect of pre-reduction on final reduction degree. ISIJ Int 2005;45(2):151–8. http://dx.doi.org/10.2355/isijinternational.45.151.
[47] Spreitzer D, Schenk J. Reduction of iron oxides with hydrogen—A review. Steel Res Int 2019;90(10). http://dx.doi.org/10.1002/srin.201900108.
[48] Habermann A. Kinetik der Eisenerzreduktion in der Wirbelschicht: Kinetik der Eisenerzreduktion in der Wirbelschicht [Ph.D. thesis], Technische Universität Wien; 2001, URL: https://repositum.tuwien.at/handle/20.500.12708/180163.
[49] Schmid JC. Development of a novel dual fluidized bed gasification system for increased fuel flexibility: development of a novel dual fluidized bed gasification system for increased fuel flexibility [Ph.D. thesis], TU Wien; 2014, http://dx.doi.org/10.34726/hss.2014.25397, URL: https://repositum.tuwien.at/handle/20.500.12708/7804.
[50] Abba IA, Grace JR, Bi HT, Thompson ML. Spanning the flow regimes: Generic fluidized–bed reactor model. AIChE J 2003;49(7):1838–48. http://dx.doi.org/10.1002/aic.690490720.
[51] MIDREX. Hotlink® system benefits of charging hot dri (HDRI). Technical report, 2014, URL: https://www.midrex.com/wp-content/uploads/Hot_Transport_-_HOTLINK.pdf.
[52] LP Patley. Properties evaluation of mild steel, medium carbon steel and high carbon steel. Technical report, 2013.
[53] Kirschen M. Visualization of slag data for efficient monitoring and improvement of steelmaking slag operation in electric arc furnaces, with a focus on MgO saturation. Metals 2021;11(1):17. http://dx.doi.org/10.3390/met11010017, URL: https://www.mdpi.com/2075-4701/11/1/17.
[54] Neuschütz D, Spirin D. Nitrogen removal and arc voltage increase in EAF steelmaking by methane injection into the arc. Steel Res Int 2003;74(1):19–25. http://dx.doi.org/10.1002/srin.200300156.
[55] Shahabuddin M, Rahbari A, Sabah S, Brooks G, Pye J, Rhamdhani MA. The performance and charge behaviour in melter/smelter for the production of hot metal in hydrogen DRI-based steelmaking. Ironmak Steelmak: Process Prod Appl 2024. http://dx.doi.org/10.1177/03019233241265179.
[56] Pfeiffer A, Schenk J, Wimmer G, Wurm J. Processing low grade direct reduced iron–definition and comparison of melting strategies. In: 9th EOSC & 6th CTSI. 2022.
[57] Madhavan N, Brooks GA, Rhamdhani MA, Rout BK, Schrama FNH, Overbosch A. General mass balance for oxygen steelmaking. Ironmak Steelmak: Process Prod Appl 2021;48(1):40–54. http://dx.doi.org/10.1080/03019233.2020.1731252.
[58] Sabah S, Shahabuddin M, Rahbari A, Brooks G, Pye J, Rhamdhani MA. Effect of gangue on CO 2 emission for different decarbonisation pathways. Ironmak Steelmak: Process Prod Appl 2024;51(4):356–68. http://dx.doi.org/10.1177/03019233241242553.
[59] Thomas C, Rosales J, Polanco JA, Agrela F. Steel slags. New Trends Eco-Efficient Recycl Concr 2019;169–90. http://dx.doi.org/10.1016/B978-0-08-102480-5.00007-5, URL: https://www.sciencedirect.com/science/article/pii/b9780081024805000075.
[60] European Hydrogen Observatory. Tools and reports: Datasets: Electrolyser cost 2024. Technical report, 2024, URL: https://observatory.clean-hydrogen.europa.eu/tools-reports/datasets.
[61] Towler G, Sinnott R. Chemical engineering design: principles, practice and economics of plant and process design. Technical report, Butterworth-Heinemann; 2021.
[62] Mills K, Yuan L, Jones R. Estimating the physical properties of slags. J South Afr Inst Min Met 2011. URL: https://www.scielo.org.za/scielo.php?pid=s2225-62532011001000002&script=sci_arttext.
[63] Echterhof T. Review on the use of alternative carbon sources in EAF steelmaking. Metals 2021;11(2):222. http://dx.doi.org/10.3390/met11020222.
[64] Ren S, Yang S, Chen H, Wang L, Liu M, Wang G, Xu C. A state-of-the-art review on the utilization of biochar as renewable energy for the sustainable steel industry. Appl Energy 2025;394:126188. http://dx.doi.org/10.1016/j.apenergy.2025.126188, URL: https://www.sciencedirect.com/science/article/pii/S0306261925009183.
[65] International Energy Agency. Achieving net zero heavy industry sectors in G7 members. Technical report, OECD Publishing; 2022.
[66] Gao M, Zhao L, Liu D, Gao J, Xu C. Research progress of electrically intensified catalytic processes: Internal resistance heating and electrical activation. 524, 2025, 169060. http://dx.doi.org/10.1016/j.cej.2025.169060, 1385-8947.
[67] ThermCraft Inc. Electrical resistance heating elements: an overview. Technical report, 2016, URL: https://thermcraftinc.com/wp-content/uploads/2018/01/Heating_Element_Seminar_Nov_2_2016.pdf.
[68] World Steel Association. Sustainability performance of the steel industry 2003–2023. Sustain Indic 2024 Rep 2024. URL: https://worldsteel.org/wp-content/uploads/Sustainability-Indicators-report-2024.pdf.
[69] Hemauer J, Rehfeldt S, Klein H, Peschel A. Performance and cost modelling taking into account the uncertainties and sensitivities of current and next-generation PEM water electrolysis technology. Int J Hydrog Energy 2023;48(66):25619–34. http://dx.doi.org/10.1016/j.ijhydene.2023.03.050.
[70] Enerdata. Forecasted CO_2 intensity of electricity generation worldwide from 2000 to 2050, by region (in grams of carbon dioxide per kilowatt hour). Technical report, 2024, URL: https://www.statista.com/statistics/1257765/global-emission-intensity-electricity-generation-region/.
[71] DBS Group Research. Forecasted hot-rolled coil (HRC) steel benchmark price worldwide for 2023 (in U.S. dollars per metric ton). Technical report, 2022, URL: https://www.statista.com/statistics/214246/world-steel-prices/.
[72] Peschel A, Wasserscheid P. Perspective on the technology status of chemical hydrogen carriers for ship–based energy import. Electrochem Sci Adv 2026;6(1). http://dx.doi.org/10.1002/elsa.70015.
[73] Johnson N, Liebreich M, Kammen DM, Ekins P, McKenna R, Staffell I. Realistic roles for hydrogen in the future energy transition. Nat Rev Clean Technol 2025;1(5):351–71. http://dx.doi.org/10.1038/s44359-025-00050-4.
[74] Devlin A, Kossen J, Goldie-Jones H, Yang A. Global green hydrogen-based steel opportunities surrounding high quality renewable energy and iron ore deposits. Nat Commun 2023;14(1):2578. http://dx.doi.org/10.1038/s41467-023-38123-2.